Industrial Engineering & Management

Trivedi et al., Ind Eng Manage 2015, 4:3
DOI: 10.4172/2169-0316.1000161

Research Article Open Access

Studies of the Atomic and Crystalline Characteristics of Ceramic Oxide Nano Powders after Bio field Treatment

Mahendra Kumar Trivedi, Gopal Nayak, Shrikant Patil*, Rama Mohan Tallapragada and Omprakash Latiyal

Trivedi Global Inc., 10624 S Eastern Avenue Suite A-969, Henderson, NV 89052, USA

Abstract

Transition metal oxides (TMOs) have been known for their extraordinary electrical and magnetic properties. In the present study, some transition metal oxides (Zinc oxide, iron oxide and copper oxide) which are widely used in the fabrication of electronic devices were selected and subjected to biofield treatment. The atomic and crystal structures of TMOs were carefully studied by Fourier transform infrared (FT-IR) spectroscopy and X-ray diffraction (XRD) studies. XRD analysis reveals that biofield treatment significantly changed the lattice strain in unit cells, crystallite sizes and densities in ceramics oxide powders. The computed molecular weight of the treated samples exhibited significant variation. FT-IR spectra indicated that biofield treatment has altered the metal-oxygen bond strength. Since biofield treatment significantly altered the crystallite size, lattice strain and bond strength, we postulate that electrical and magnetic properties in TMOs (transition metal oxides) can be modulated by biofield treatment.

Keywords: Biofield treatment; Iron oxide; Copper oxide; Zinc oxide; X-ray diffraction; FT-IR

Introduction

Transition metal oxides (TMOs) exhibit fascinating properties such as piezoelectricity, ferroelectricity, nonlinear optical behaviour, wide band gap and high-TC superconductivity, which allows these metal oxides to use in electronic and optical device industries [1]. Zinc oxide (ZnO) is a common example of TMO which has been used in fabrication of light emitting diodes (LEDs), Varistors (a ceramic resistor which used to protect electronic circuits from high voltages) due to its wide band gap (3.37eV) and large excitation binding energy [2-4]. On the other hand iron oxide (Fe_3O_4) is mainly utilized in fabrication of biosensors due to its low inherent toxicity, biocompatibility and strong paramagnetic behaviour [5]. Copper oxide has been used as a p-type semiconductor for the fabrication of electrical, photovoltaic devices, field emission devices due to its narrow band gap of 1.5 eV and high optical absorption coefficient [6]. Moreover, in TMOs the magnetic, electrical and optical properties are directly influenced by lattice strain and crystallite size [7,8].

ZnO using in Varistors requires low leakage current during continuous operating voltage and uniform current distribution for better performance, which is possible by controlling its crystallite size [7]. Energy band gaps in ZnO and CuO can be controlled by increasing or decreasing the lattice parameter (Energy band gap is inversely proportional to lattice parameter) [8]. Researchers have optimized band gap in ceramics by controlling the composition of certain alloys and lattice constant of unit cell. It is known that tailoring the energy band gap in ceramic oxides is crucial to create barrier layers and quantum wells with materials of matching properties such as electron affinity and lattice constant [9,10]. Recently, TMOs nanoparticles are synthesized by electrophoretic deposition, laser ablation, anodization hydrothermal methods, electrochemical depositions sol–gel method, microwave-assisted combustion chemical vapour deposition, thermal decomposition, combustion method, ultrasound method and co-precipitation as per various literatures, wherein correlation of band gap with crystal structure and morphology has been studied [11-21].

In the prior published studies, Biofield treatment has been used to cause the changes in the atomic and structural properties such as lattice constant, bond strength, and molecular weight. Recently it was reported that a robotic quad copter in space can be controlled through the power of thoughts [22]. Trivedi's biofield, referred herein as biofield treatment, is known to transform the atomic, molecular, structural properties of various metals and ceramics in the field of material science [23-30], such as it has enlarged the particle size by 432% in zinc powder [23] and enhanced the crystallite size by 66% in vanadium pentoxide [27]. Additionally, the biofield treatment also achieved excellent results in various other fields such as microbiology [31-33], biotechnology [34,35] and agriculture [36-38] etc., which are reported elsewhere.

In the present investigation effect of Trivedi's biofield treatment on three TMOs nanopowders, (Zinc oxide, Iron oxide and copper oxide) are studied at the atomic and structural level.

Experimental Procedure

Iron oxide, copper oxide and zinc oxide nanopowders used in the present investigation were procured from Sigma Aldrich which had purity of around 99% which were distributed into three sets, out of which one set was considered as control. And other two sets of each oxide were exposed to Mr. Trivedi's biofield, referred hereinafter as treated T1 and treated T2.

All samples were characterized by X-ray diffraction (XRD) Phillips, Holland PW 1710 with copper anode, nickel filter and radiation of wavelength of 1.54056 Å. XRD evaluated result was obtained in the form of intensity vs. 2θ with a table containing d values, 2θ°, peak width 2θ°, relative Intensity %, peak intensity counts, etc. For data analysis, Standard JCPDS database and Miller indices h, k, l were used to get the value of "d" and Powder X software was used to calculate lattice

***Corresponding author:** Shrikant Patil, Trivedi Global Inc., 10624 S Eastern Avenue Suite A-969, Henderson, NV 89052, USA, Tel: +1 602-531-5400; E-mail: publication@trivedieffect.com

Received April 23, 2015; **Accepted** June 15, 2015; **Published** June 17, 2015

Citation: Trivedi MK, Nayak G, Patil S, Tallapragada RM, Latiyal O (2015) Studies of the Atomic and Crystalline Characteristics of Ceramic Oxide Nano Powders after Bio field Treatment. Ind Eng Manage 4: 161. doi:10.4172/2169-0316.1000161

parameter and unit cell volume. Crystallite size (size of a grain) was computed as:

Crystallite size=k λ/b Cos θ

Here λ is the wavelength of x-radiation k is the equipment constant with a value 0.94.

Percent change in unit cell volume was calculated as 100 × (ΔV/V_c) where ΔV=[(V_t-V_c)/V_c] where V_t and V_c are the unit cell volume of treated and control samples respectively. Similarly percent change in lattice parameter, molecular weight, density was computed. The atomic weight of an atom is calculated as the sum of weights of all protons, neutron and electron present in an atom and molecular weight was calculated as the sum of atomic weights of all atoms present in a molecule. Density was calculated as molecular weight multiplied by number of molecules in a unit cell divided by unit cell volume.

The infrared spectra of metal oxide powders were carried out using with Perkin Elmer, USA Fourier Transform Infrared (FT-IR) Spectrometer, which recorded data in the range of 500-4000/cm.

Results and Discussion

X-ray diffraction (XRD)

Figure 1 shows the comparative results of lattice parameter 'a' of various control and treated ceramic nanopowders with the values obtained from standard JCPDS (Joint Committee on Powder Diffraction Standards) data. It was found that the value of lattice parameter "a" of control powder was closely matched with the standard JCPDS values. However in case of treated nanopowder samples, the biofield treatment has induced changes in lattice parameter to second decimal place (Table 1).

The percent variation in lattice parameter of treated samples is shown in Figure 2. It was observed that the lattice parameter was significantly decreased by 0.6%, 0.39% and 0.04% in Fe_3O_4, CuO, and ZnO powders, respectively. The volume of the unit cell was calculated using the parameter 'a' that showed similar variation as given in Table 1. The decrease in lattice parameters of all the treated powders indicated that a compressive stress has been applied through biofield treatment. The percent change in linear strain (100 × (Δa/a_c) would be significant, if it's value is above 0.2% ,which is considered to be above the elastic limit. Once applied stress over unit cell is removed, the elastic strain is expected to release, which did not happen in present investigation. Rather the strain was permanent, which revealed that it is plastic by nature, but the ceramics are elastic materials [39,40]. The absence of dislocations in covalent ceramics and the narrow dislocation width in ionic ceramics make this exhibit elastic behavior.

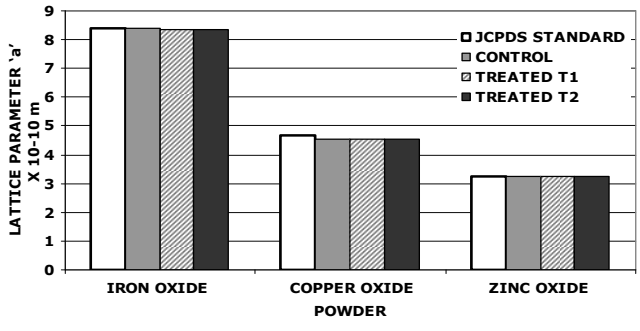

Figure 1: Comparison of lattice parameter 'a' of treated ceramic nanopowders with standard JCPDS data and control.

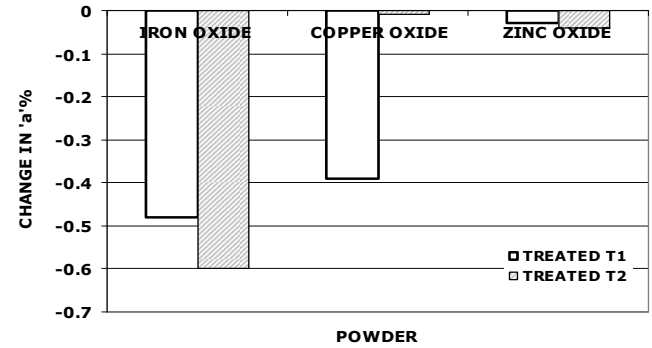

Figure 2: Percent change in lattice parameter 'a' between control and treated ceramic nanopowders.

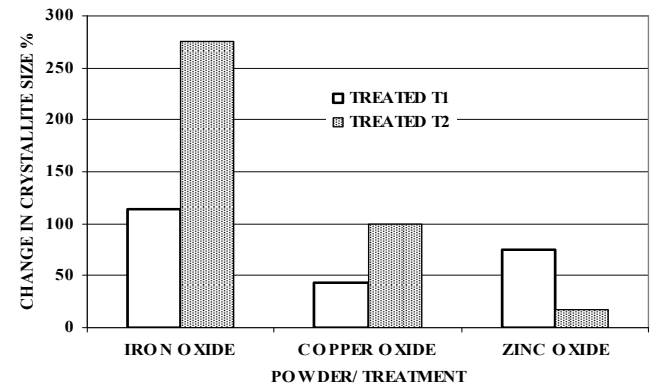

Figure 3: Percent change crystallite size between control and treated powders.

The percent changes in crystallite size are presented in Figure 3. In treated samples, it was found that the crystallite size was significantly increased up to 275.26%, 98.92% and 77.7% in Fe_3O_4, CuO, and ZnO powders, respectively. The higher crystallite size in treated samples suggests heavy plastic deformation along with large expansion and growth.

The ceramics are elastic material, and their dislocation concentration is minimal. Furthermore high energy is required to move the dislocations in ceramic crystals than crack propagation; hence ceramics fails by brittle fracture rather than plastic deformation. The results showed that ceramic crystallite size was increased, may be due to re-crystallization and crystallite growth which might have been possible in the presence of large amount of energy (localized heat to at least above one third of melting point) in the crystals, provided by the biofield treatment. Another reason may be the rotation of crystallites at their boundaries aided by viscous flow which has been known to occur in nano crystalline solids. Whatever be the mechanism the decrease in lattice parameters and increase in crystallite size are opposing effects, which is an unusual phenomena. So it is necessary to study the characteristics at the atomic level.

The lattice parameters are considered as the equilibrium inter atomic distance where the attractive forces of nuclear charges of metal ions are balanced by the negative charges of metal ions. The effective nuclear charge on the metal ion was reduced with increasing distance from the nucleus. When compressive force has been applied over atoms then electron clouds are likely to be pushed toward the nucleus,

	IRON OXIDE Fe3O4 82-1533 CUBIC	COPPER OXIDE CuO 80—1917 MONOCLINIC	ZINC OXIDE ZnO 80-0075 HEXAGONAL	IRON OXIDE Fe3O4 82-1533 CUBIC	COPPER OXIDE CuO 80—1917 MONOCLINIC	ZINC OXIDE ZnO 80-0075 HEXAGONAL
	LATTICE PARAMETER 'a' × 10^{-8} cm			% CHANGE IN 'a'		
JCPDS Standard	8.397	4.688	3.254			
Control	8.387	4.541	3.254			
Treated T1	8.347	4.524	3.2529	-0.48	-0.39	-0.03
Treated T2	8.337	4.541	3.2527	-0.60	-0.01	-0.04
	VOLUME OF UNIT CELL × 10^{-24} Cm			% CHANGE IN VOLUME OF UNIT CELL		
Control	589.99.	804.99	47.729			
Treated T1	581.48	805.53	47.759	-1.44	0.07	-0.06
Treated T2	579.42	805.31	47.768	-1.79	0.04	-0.07
	CRYSTALLITE SIZE 'G' × 10^{-9} m			% CHANGE IN 'G'		
Control	28.95	43.44	61.87			
Treated T1	62.09	62.07	108.27	114.46	42.87	74.99
Treated T2	108.65	86.88	72.18	275.26	100.00	16.66

Table 1: Analysis of X-ray diffraction results of oxide nano powders-crystal parameters.

	IRON OXIDE Fe_3O_4	COPPER OXIDE CuO	ZINC OXIDE ZnO	IRON OXIDE Fe_3O_4	COPPER OXIDE CuO	ZINC OXIDE ZnO
	Molecular Weight (Weight of Number Of Neutrons And Protons) g/g. mol			% Change In Molecular Weight (Percent Change In Weight of Number Of Neutrons And Protons)		
Control	233.99	80.69	81.70			
Treated T1	230.61	80.74	81.75	-1.443	0.067	0.063
Treated T2	229.80	80.72	81.76	-1.793	0.040	0.082
	DENSITY g/cc			% Change In Density		
Control	5.268	6.657	5.684			
Treated T1	5.345	6.652	5.687	1.465	-0.067	0.062
Treated T2	5.364	6.654	5.688	1.826	-0.040	0.074

Table 2: Analysis of X-ray diffraction results of oxide nano powders-molecular weight and density.

that lead to further reduction in the size of the atoms and cause an increase in the nuclear charge per unit volume, whereas reverse may happen in case of tensile stress. The calculated values of the atomic parameters and their percentage variation between control and treated samples are given in Tables 1 and 2 and Figures 4-6. It was observed that unit cell volume was decreased in iron oxide and zinc oxide due to decrease in lattice parameter "a". Contrarily the unit cell volume was increased in copper oxide due to increase in lattice parameter "c". Furthermore, the change in unit cell volume affects the size of atom that changes the effective nuclear charge per unit volume of the metal ions accordingly. The observed decrease in molecular weight and density was mainly attributed to the change in proton to neutron ratio inside the nucleus. This could be due to weak reversible nuclear level reaction, which occurred inside the nucleus. Thus, we presume that biofield has transferred the energy in the form of neutrinos that possibly caused this nuclear level reaction to alter their ratio. Furthermore, it is already reported that the crystallite size and lattice strain in ceramic nano oxides directly affects the energy band gap and piezoelectric properties. The higher crystallite size indicates lower energy band gap, which make these oxides more useful in semiconductors [6,9].

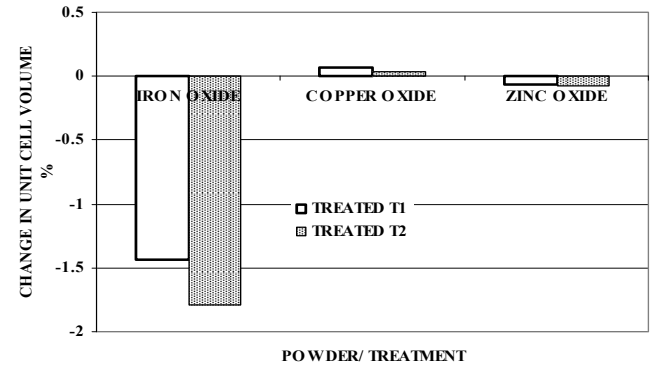

Figure 4: Percent change in unit cell volume between control and treated ceramic nanopowders.

FT-IR spectroscopy

FT-IR spectrum of zinc oxide (control) and treated sample is illustrated in Figure 7. FT-IR of the zinc oxide (control) exhibited absorption peaks at 547/cm, 496/cm and 440/cm, which were attributed to the characteristic Zn-O stretching vibrations peaks [41]. Whereas treated sample of zinc oxide showed an emergence of a broad peak at 3410/cm which was responsible for O-H stretching vibrations. Here, we presume that biofield treatment is responsible for increasing the surface to volume ratio of ZnO leading to enhanced moisture absorption [42,43] by the treated sample. Other important peaks were observed at 425/cm, 547/cm could be ascribed to Zn-O stretching vibration, and absorption peaks at 878/cm and 1275/cm corresponds to H-O-H and O-H bending vibration, respectively [42]. The absorption band of control and treated sample of ZnO was observed at 440/cm and 425/cm, respectively. The treated ZnO sample showed lower wavenumber (425/cm), that may be due to unit cell distortion or change in Zn—O bond length [44].

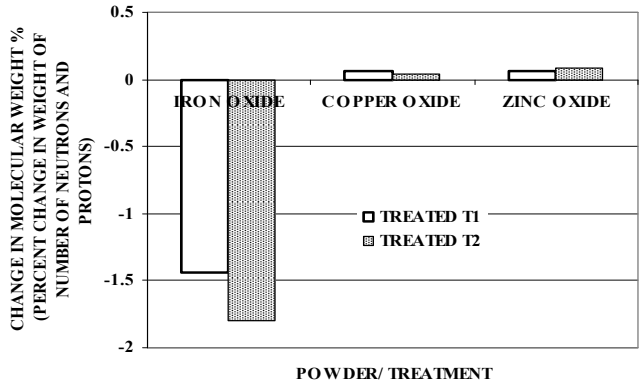

Figure 5: Percent change in molecular weight (Change in weight of total number of protons and neutrons) of treated ceramic nanopowders.

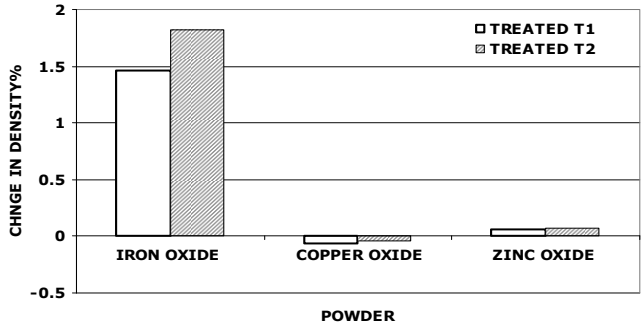

Figure 6: Percentage change in density of control and treated ceramic nanopowders.

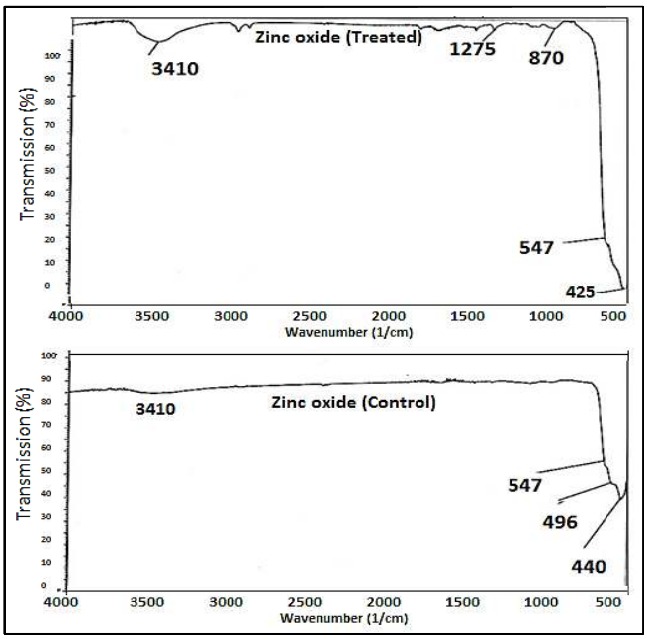

Figure 7: FT-IR spectrum of control and treated samples of zinc oxide.

FT-IR spectrum of copper oxide is shown in Figure 8. The FT-IR of copper oxide (control) has showed only one peak at 619/cm, which was mainly due to Cu (II)-O stretching vibrations peak [45]. Contrarily

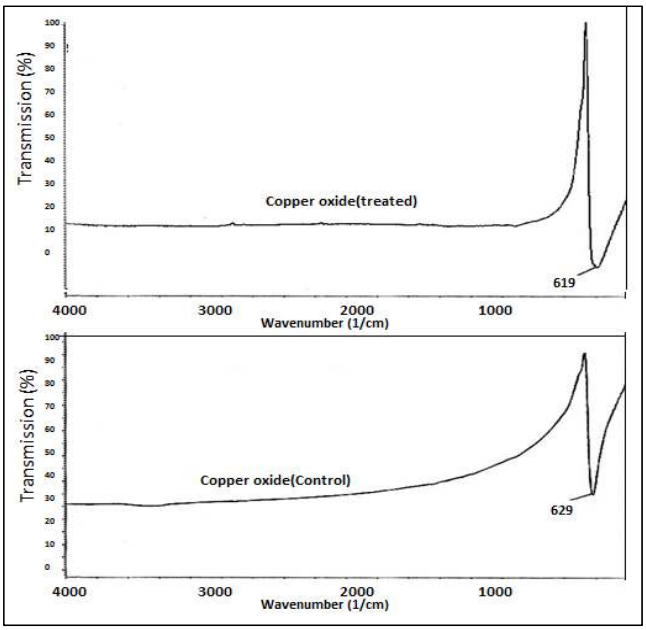

Figure 8: FT-IR spectrum of control and treated samples of copper oxide.

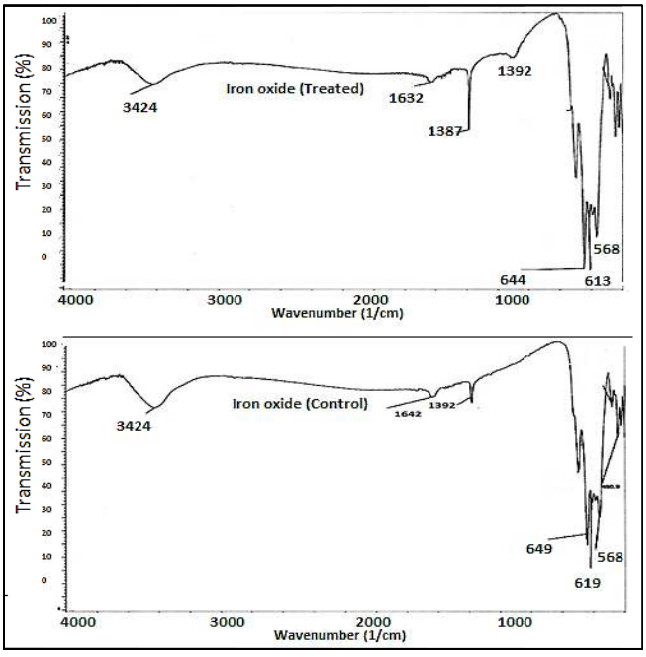

Figure 9: FT-IR spectrum of control and treated samples of iron oxide.

in treated copper oxide sample, this absorption peak was observed at higher wavenumber, 629/cm that may have been due to a reduction in particle size or strengthening of Cu—O bond through biofield treatment [46].

The FT-IR spectrum of Iron oxide is illustrated in Figure 9. The Iron oxide (control) sample showed intense absorptions peaks at 619/cm and 568/cm respectively which could be due to Fe-O stretching vibrations in Fe_3O_4 [47]. The treated iron oxide sample exhibited peaks at 644.4/cm and 568/cm respectively which were attributed to the Fe—O vibration peaks [47,48]. This may be due to contributions

from the stretching vibration bands related to metal in the tetrahedral and octahedral sites of the oxide structure. However in treated Fe_3O_4, the absorption band responsible for Fe-O bond shifted towards higher wavenumber of 644/cm, which may be possible due to breaking of many bonds on surface atoms. This may cause rearrangement of localized electrons on the particle surface leading to increase in surface bond force constant; followed by the shifting of absorption bands to higher wavenumber [49]. It is hypothesized that energy through biofield treatment has been transferred to atoms, which caused these changes in bond properties.

In present work, biofield treatment altered the atomic and structural properties, which may lead to the changes in corresponding optical and electrical properties in ceramic nanopowders.

Conclusion

Biofield treatment by Mr. Trivedi has significantly altered the atomic and crystalline characteristics of nano Iron oxide (Fe_3O_4), nano copper oxide (CuO) and nano zinc oxide (ZnO) as follows;

- As per the results, the decrease in volume of unit cell up to 1.79% and an increase in crystallite size by 275.26% are opposing effects and can be only explained based on current knowledge in terms of dislocation movements during recovery and re-crystallization. This is an unprecedented phenomenon observed, since ceramics are elastic solids.
- The treated powders exhibited increase as well decrease in volume of the unit cell and molecular weight. The changes in density are exactly reversed. This inverse relationship between density and molecular weight can only be explained by changes in the total number of neutrons and protons as well as their ratio. So we hypothesize that the results achieved could be due to changes in protons and neutrons in the nucleus caused by weak interactions.
- FT-IR spectra showed, significant shifting of M-O stretching vibration in all transition metal oxides (TMOs), which revealed that biofield treatment have altered the bond length and bond force constant.
- Based on the higher crystallite size and higher lattice strain achieved in treated ZnO, Fe_3O_4 and CuO powders ; we assume that these ceramics could be used for piezoelectric devices, ferrofluids, and semiconductor applications, respectively.

Acknowledgement

We sincerely thank to all the laboratory staff of various laboratories for their active support in characterizing the samples. We thank Dr. Cheng Dong of NLSC, Institute of Physics, and Chinese Academy of Sciences for permitting us to use PowderX software for analyzing XRD results.

References

1. Cox PA (1992) Transition Metal Oxides: An Introduction to their Electronic Structure and Properties. Oxford University Press.
2. Fan JC, Chang SL, Xie Z (2013) Optoelectronics-Advanced Materials and Devices: ZnO-Based Light-Emitting Diodes, China Hunan University. Pub Intech.
3. Meshkatoddini MR (2011) Metal Oxide ZnO-Based Varistor Ceramics. Pub Intech.
4. Chaari M, Matoussi A, Fakhfakh Z (2011) Structural and Dielectric Properties of Sintering Zinc Oxide Bulk Ceramic. Materials Sciences and Application 2: 765-770.
5. Loh KS, Lee YH, Musa A, Salmah AA, Zamri I (2008) Use of Fe_3O_4 nanoparticles for enhancement of biosensor response to the herbicide 2, 4-dichlorophenoxyacetic acid. Sensors 8: 5775-5791.
6. Benramache S, Arif A, Belahssen O, Guettaf A (2013) A Study on the correlation between crystallite size and optical gap energy of doped ZnO thin film. Journal of Nanostructure in Chemistry 3: 80-85.
7. Umar A, Vaseem M, Hahn YB (2010) Growth, Properties, and Applications of Copper Oxide and Nickel Oxide/Hydroxide Nanostructures. American Scientific Publishers 2: 1-39.
8. Hanada T (2009) Basic Properties of ZnO, GaN, and Related Materials. American Scientific Publishers 1: 1-18.
9. Janotti A, Walle VD (2009) Fundamentals of zinc oxide as a semiconductor. Reports on Progress in Physics 72: 1-29.
10. Özgür Ü, Alivov C, Liu C, Teke A, Reshchikov A et al. (2005) A comprehensive review of ZnO materials and devices. Applied Physics 98.
11. Kumar SS, Venkateswarlu P, Rao VR, Rao GN (2013) Synthesis, characterization and optical properties of zinc oxide nanoparticles. International Nano Letters 3: 30-35.
12. Scarisoreanu N, Metai DG, Dinescu G, Epurescu G, Ghica C et al. (2005) Properties of ZnO thin films prepared by radio-frequency plasma beam assisted laser ablation. Applied Surface Science 247: 518-525.
13. Ni YH, Wei XW, Hong JM, Ye Y (2005) Hydrothermal synthesis and optical properties of ZnO nanorods. Materials Science and Engineering 121: 42-47.
14. Chang SS, Yoon SO, Park HJ, Sakai A (2002) Luminescence properties of Zn nanowires prepared by electrochemical etching. Materials Letters 53: 432-436.
15. Ristiac M, Musiac S, Ivanda M, Popoviac S (2005) Sol-gel synthesis and characterization of nanocrystalline ZnO powders. Journal of Alloys and Compounds 397: L1-L4.
16. Wu JJ, Liu SC (2002) Low-temperature growth of well-aligned ZnO nanorods by chemical vapor deposition. Advanced Materials 14: 215-218.
17. Wang RC, Tsai CC (2009) Efficient synthesis of ZnO nanoparticles, nanowalls, and nanowires by thermal decomposition of zinc acetate at a low temperature. Applied Physics A 94: 241-245.
18. Lamas DG, Lascalea GE, Walsoc NE (1998) Synthesis and characterization of nano crystalline powders for partially stabilized zirconia ceramics. Journal of the European Ceramic Society 18: 1217-1221.
19. Badhuri S, Badhuri SB (1997) Enhanced low temperature toughness of Al_2O_3-ZrO_2 nano/nano composites. Nanostructured Materials 8: 755-763.
20. Khorsand Z, Abid A, Majid WH, Wang HZ, Yousefi R et al. (2013) Sonochemical synthesis of hierarchical ZnO nanostructures. Ultrasonics Sonochemistry 20: 395-400.
21. Kooti M, Sedish N (2013) Microwave-assisted combustion synthesis of ZnO nanoparticles. Journal of Chemistry 2013: 1-4.
22. LaFleur K, Cassady K, Doud A, Shades K, Rogin E et al. (2013) Quadcopter control in three dimensional space using a non-invasive motor imagery-based brain-computer interface. Journal of Neural Engineering 10: 1-15.
23. Trivedi MK, Tallapragada RR (2008) A transcendental to changing metal powder characteristics. Metal Powder Report 63: 22-28, 31.
24. Dabhade VV, Tallapragada RR, Trivedi MK (2009) Effect of external energy on atomic, crystalline and powder characteristics of antimony and bismuth powders. Bulletin of Materials Science 32: 471-479.
25. Trivedi MK, Tallapragada RR (2009) Effect of super consciousness external energy on atomic, crystalline and powder characteristics of carbon allotrope powders. Materials Research Innovations 13: 473-480.
26. Trivedi MK, Patil S, Tallapragada RM (2012) Thought Intervention through Biofield Changing Metal Powder Characteristics Experiments on Powder Characterisation at a PM Plant. Springer Berlin Heidelberg 173: 247-252.
27. Trivedi MK, Patil S, Tallapragada RM (2013) Effect of Biofield Treatment on the Physical and Thermal Characteristics of Vanadium Pentoxide Powders. Journal of Material Sciences and Engineering S11:001.
28. Trivedi MK, Patil S, Tallapragada RM (2013) Effect of bio field treatment on the physical and thermal characteristics of Silicon, Tin and Lead powders. Journal of Material Sciences and Engineering 2: 125.

29. Trivedi MK, Patil S, Tallapragada RM (2014) Atomic, Crystalline and Powder Characteristics of Treated Zirconia and Silica Powders. Journal of Material Sciences and Engineering 3: 144.

30. Trivedi MK, Patil S, Tallapragada RM (2015) Effect of Biofield Treatment on the Physical and Thermal Characteristics of Aluminium Powders. Industrial Engineering and Management 4:151.

31. Trivedi MK, Patil S (2008) Impact of an external energy on Staphylococcus epidermis [ATCC -13518] in relation to antibiotic susceptibility and biochemical reactions-An experimental study. Journal of Accord Integrative Medicine 4: 230-235.

32. Trivedi M, Patil S (2008) Impact of an external energy on Yersinia enterocolitica [ATCC -23715] in relation to antibiotic susceptibility and biochemical reactions: An experimental study. The Internet Journal of Alternative Medicine 6.

33. Trivedi M, Bhardwaj Y, Patil S, Shettigar H, Bulbule A (2009) Impact of an external energy on Enterococcus faecalis [ATCC-51299] in relation to antibiotic susceptibility and biochemical reactions-An experimental study. Journal of Accord Integrative Medicine 5: 119-130.

34. Patil SA, Nayak GB, Barve SS, Tembe RP, Khan RR (2012) Impact of Biofield Treatment on Growth and Anatomical Characteristics of Pogostemon cablin (Benth.). Biotechnology 11: 154-162.

35. Altekar N, Nayak G (2015) Effect of biofield treatment on plant growth and adaptation. Journal of Environment and Health sciences 1: 1-9.

36. Shinde V, Sances F, Patil S, Spence A (2012) Impact of Biofield Treatment on Growth and Yield of Lettuce and Tomato. Australian Journal of Basic and Applied Sciences 6: 100-105.

37. Sances F, Flora E, Patil S, Spence A, Shinde V (2013) Impact of Biofield Treatment on Ginseng and Organic Blueberry Yield. AGRIVITA, Journal of Agricultural Science 35: 1991-8178.

38. Lenssen AW (2013) Biofield and Fungicide Seed Treatment Influences on Soybean Productivity, Seed Quality and Weed Community. Agricultural Journal 8: 138-143.

39. Wang F, Gou W, Zheng X, Lu M (1998) Effective elastic moduli of ceramics with pores. Journal of Materials Science and Technology 14: 286-288.

40. Meza LR, Das S, Greer JR (2014) Strong, Lightweight, and recoverable three-dimensional ceramic nano lattices. Sciencemag 345: 1322-1326.

41. Rao CNR (1963) Chemical Applications of Infrared spectroscopy. Academic Press. New York and London.

42. Čepin M, Hribar G, Caserman S, Orel ZC (2015) Morphological impact of zinc oxide particles on the antibacterial activity and human epithelia toxicity. Material Sciences and Engineering 52: 204-211.

43. Kumar D, Reddy LS (2014) Antibacterial and photo catalytic activities of ZnO Nanoparticles: Synthesis via combustion method. International Journal of Engineering and Technology 3: 2278-2540.

44. Dutta S, Ganguly BN (2010) Characterization of ZnO nanoparticles grown in presence of Folic acid template. Nanobiotechnology 10: 29-39.

45. Radhakrishnan AA, Beena BB (2014) Structural and Optical Absorption Analysis of CuO Nanoparticles. Indian Journal of Advances in Chemical Science 2: 158-161.

46. Varughese G, Rini V, Suraj SP, Usha KP (2014) Characterisation and optical studies of copper oxide nanostructures doped with lanthanum ions. Advances in materials science 14: 49-60.

47. Yousefi M, Alimard P (2013) Synthesis of M-Nd doped Fe_3O_4 nanoparticles (M=Co, Ce, Cr, Ni) with tunable magnetic properties. Bulletin of the Chemical Society of Ethiopia 27: 49-56.

48. Lopez JA, Flavio FG (2010) Synthesis and characterization of Fe_3O_4 magnetic nanofluid. Revised Latinoamericana de Metalurgiay Materiales 30: 60-66.

49. Sundrarajan M, Ramalakshmi M (2011) Novel Cubic Magnetite Nanoparticle Synthesis Using Room Temperature Ionic Liquid. Journal of Chemistry 9: 1070-1076.